AIP Journal of Applied Physics

Millisecond non-melt laser annealing of phosphorus implanted germanium: Influence of nitrogen co-doping

S. Stathopoulos, L. Tsetseris, N. Pradhan, B. Colombeau, and D. Tsoukalas

Citation: Journal of Applied Physics **118**, 135710 (2015); doi: 10.1063/1.4932600
View online: http://dx.doi.org/10.1063/1.4932600
View Table of Contents: http://scitation.aip.org/content/aip/journal/jap/118/13?ver=pdfcov
Published by the AIP Publishing

Millisecond non-melt laser annealing of phosphorus implanted germanium: Influence of nitrogen co-doping

S. Stathopoulos,[1] L. Tsetseris,[1] N. Pradhan,[2] B. Colombeau,[2] and D. Tsoukalas[1]
[1]*Department of Physics, National Technical University of Athens, Zografou, Athens 15773, Greece*
[2]*Applied Materials—Varian, Gloucester, Massachusetts 01930, USA*

(Received 27 July 2015; accepted 25 September 2015; published online 7 October 2015)

In this work, we present the results obtained using a CO_2 laser source at 10.6 μm wavelength for the study of the non-melt annealing of phosphorus doped germanium in the millisecond regime. Main objective of this paper is the demonstration of electrically active n^+-p junctions in germanium by implanting phosphorus in p-type substrate while trying to maintain minimal dopant diffusion, which is a critical issue for scaling germanium devices. In addition to the phosphorus diffusion studies, we also explore the presence of nitrogen introduced in the substrate together with phosphorus and we conclude that it can further reduce dopant movement at the expense of lower activation level. The observation is confirmed by both electrical and SIMS measurements. Moreover, density functional theory calculations show that nitrogen-phosphorus co-doping of germanium creates stable N-P complexes that, indeed, are consistent with the deactivation and diffusion suppression of phosphorus.
 [http://dx.doi.org/10.1063/1.4932600]

I. INTRODUCTION

As the silicon nodes approach the end of scaling, alternative methods and processes for the development of the next generation of nanoelectronic devices are explored. These include either new transistor architectures and/or new substrate materials. As far as the latter is concerned, out of the breadth of available materials, germanium seems a viable candidate since it has a series of competitive advantages such as high mobility for both electrons and holes and is highly compatible with the current silicon processing technology. However, the fabrication of shallow junctions in p-type germanium substrates is still significantly challenging mainly due to the highly mobile n-type dopants. The diffusion coefficients of the most common n-type dopants (phosphorus, antimony, and arsenic) are very high in stark contrast to p-type dopants such as boron and gallium whose diffusion coefficient is several orders of magnitude lower.[1–3] Additionally, it has been observed[4] that there is a significant substrate loss during regular thermal annealing cycles used to activate the implanted dopants an effect that is correlated with annealing ambient conditions.[5] This issue requires the use of additional dielectric capping layer to prevent the induced dose loss.

The approach proposed by this paper to confront these issues is twofold; first, we are using a CO_2 laser source at 10.6 μm in the millisecond range in order to provide a high thermal budget within a short period (10 ms or less) while remaining in the sub-melt regime. The same setup has been previously used by the authors[6] with promising results in the formation of ultra shallow junctions in silicon. Laser annealing is a common technique to electrically activate carriers in semiconductors with promising results in germanium,[7,8] and deep infrared CO_2 lasers also have the added benefit of reducing pattern dependency when operated in Brewster's angle.[9] Second, we investigate the co-doping of the substrate with nitrogen (N_2^+) and its effect in retarding the diffusion of phosphorus. The effect of nitrogen has been previously demonstrated originally by Simoen *et al.*[10] and more recently by Thomidis *et al.*[11] to be beneficial in limiting the fast diffusion of phosphorus in germanium (fluorine has also been shown to have a similar effect[12]) and is also confirmed by this paper. Additionally, we investigate the effect of P-N binding as the mechanism of diffusion and activation suppression of phosphorus dopants in germanium through density-functional theory (DFT) calculations and assess the results through SIMS and sheet resistance measurements.

II. EXPERIMENTAL PROCEDURE

Two different sets of samples have been prepared all using p-type germanium substrates with 2 to 5 Ω cm resistivity cut into $0.8 \times 0.8\,cm^2$ pieces. A 32 nm thick RF sputtered SiO_2 film has been deposited at 200 °C, where a $600 \times 600\,\mu m^2$ window has been etched using optical lithography. This limits the introduction of ions by the subsequent ion implantations in this area thus creating a very steep dopant concentration gradient that aids us during electrical characterization by limiting the side leakage. In order to ensure that the implant tail will not penetrate the SiO_2 film, the 1 μm thick photoresist was not removed until after the implantation. Then, all samples have been implanted with phosphorus ions at 30 keV energy and $1 \times 10^{15}\,cm^{-2}$ dose. The first set of samples was left as is, while the second set of samples has seen an additional implantation step using molecular nitrogen ions (N_2^+) at the same implantation conditions as phosphorus (30 keV−$1 \times 10^{15}\,cm^{-2}$). After the implantation process, the remaining photoresist was stripped and all samples have been irradiated with our laser setup. Details for the laser setup used can be found in a previous publication.[13] The power density used was about 5500 W cm^{-2} and the pulse duration was ranging from 8 to 10 ms. Longer pulses have also been tested but have led to

considerable diffusion to be of any interest. Since germanium is transparent in far infrared at room temperature, the samples were resting vertically upon a heating base. Preheating is necessary to increase the radiation absorption rate at the beginning of the process. The preheating temperature of the samples was 270 °C for a total duration of 30–40 s, which was deemed enough to aid the absorption of the radiation. Higher preheating temperatures led to consistently higher temperatures past the melting point of germanium after being irradiated. The spot size of the beam was measured to be 1.2 mm in diameter completely covering the exposed germanium window. In all the irradiations, the maximum temperature, measured by real time infrared pyrometry, was ranging from 750 °C to 800 °C (±25 °C), well below the melting threshold of germanium. Also, for comparison purposes, an additional sample annealed at 650 °C for 30 min on a regular furnace was prepared. The sample was capped with an additional 30 nm RF sputtered SiO_2 to prevent substrate loss during the annealing.

To electrically characterize the samples, 4-point probe van der Pauw measurements have been performed. For that purpose, $100 \times 100\ \mu m^2$ gold contacts 35 nm thick with 5 nm titanium as adhesion layer and arranged in square geometry 150 μm apart have been fabricated using e-gun evaporation and the lift-off process. All contacts lie within the $600 \times 600\ \mu m^2$ window etched into the SiO_2 film and totally cover the annealed area. Since the laser beam has a Gaussian profile, the resultant doping profile is non uniform across the annealed area. So, a comprehensive sheet resistance mapping must be made in order to determine the lowest sheet resistance and, consequently, the maximum diffusion. In addition to the selective doping process illustrated, a deep circular cut with a diamond stylus has been made to further ensure the electrical isolation of the annealed area from the neighboring regions. Additionally, in order to measure the performance of the junction as a diode, a substrate wide contact has been fabricated on the backside of the sample to serve as the back contact of the diode. Experiments are concluded with SIMS for doping concentration evaluation and AFM for surface topography. SIMS measurements were performed in the area where sheet resistance was measured to be minimum.

III. RESULTS AND DISCUSSION

First, we discuss the results obtained using the samples that are implanted only with phosphorus. In Figure 1, the dopant profile for the 8 ms and 10 ms cases can be observed. The junction depth, measured at $1 \times 10^{18}\,cm^{-3}$, is determined to be about 162 nm and 200 nm for the 8 ms and 10 ms cases, respectively (Table I). For comparison, the furnace annealed sample has a junction depth well beyond the 250 nm mark. Comparing to the as-implanted profile, the net movement of the dopants ranges from 20 to 80 nm while the dose loss is small (9%) for the 8 ms case but more considerable for the 10 ms one (27%). However, both losses are quite less than the one measured for the furnace anneal (52%). The apparent "kink" at 75–80 nm is attributed to the crystalline/amorphous interface as evidenced by TEM shown in Fig. 1 of the work by Tsouroutas *et al.*[14] who have used the same phosphorus implantation conditions.

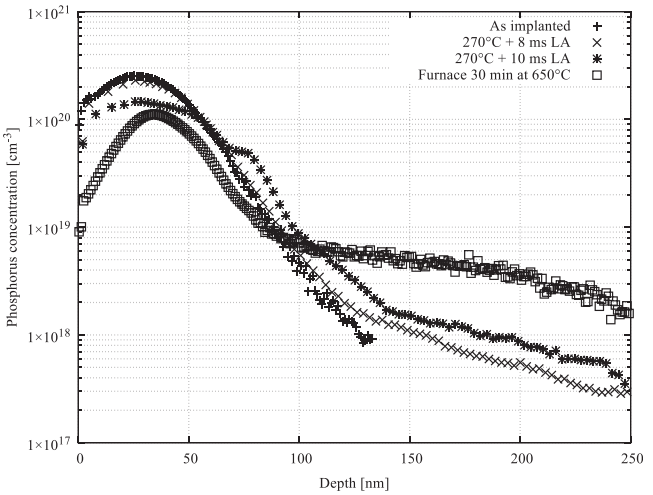

FIG. 1. SIMS dopant profile for the samples implanted only with phosphorus for 8 and 10 ms. Furnace anneal is presented for comparison.

Although millisecond annealing presented above seems well suited to control the excess diffusion of phosphorus, the use of nitrogen as a co-doping agent seems to improve the situation even more. In Figure 2, we can see the SIMS phosphorus dopant profile for the annealed samples doped with both phosphorus and nitrogen as well as for both the as-implanted and furnace annealed samples for comparison. In Figure 3, the corresponding nitrogen profiles are presented as well. The phosphorus junction depths for both the 8 and 10 ms annealed samples are both less than 140 nm corresponding to a net dopant profile movement less than 10 nm while maintaining most of the dose intact (less than 5% dose loss for both cases), which is a significant improvement over both the phosphorus-only doping and the furnace annealing. So, it is apparent that the nitrogen co-doping effectively assists in deterring the excessive diffusion of the phosphorus dopants giving us practically diffusionless junctions. As for the nitrogen profile there is minimal diffusion at the 8 ms case but slightly more pronounced for the 10 ms one. Most of the nitrogen dose is preserved with less than 2% dose loss for the 8 ms case and about 8% for the 10 ms one. The lack of significant diffusion and dope loss in the nitrogen profile indicates that nitrogen is mostly immobile. This is similar to the observations made by Thomidis *et al.*[11] for samples annealed with RTA and similar doping strategy.

As far as the sheet resistance is concerned, multiple four point probe measurements have been performed on all samples, and the results are summarized in Table II. As the table indicates, longer pulses lead to lower resistances that can be

TABLE I. Post-annealing junction characteristics. Junction depths are measured at $1 \times 10^{18}\,cm^{-3}$ doping level.

Doping	Pulse (ms)	x_j (nm)	Dose loss (%)
P only	8	162	9
P only	10	200	27
P and N_2	8	135	<5
P and N_2	10	139	<5
P only	30 min–650 °C	> 250	52

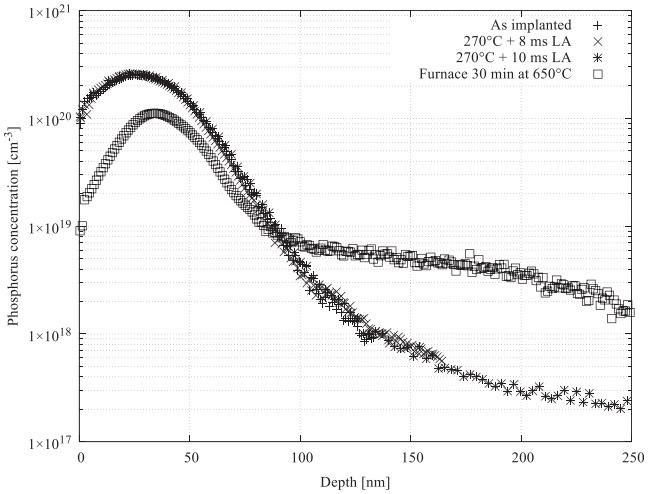

FIG. 2. SIMS dopant profile for the samples implanted with both phosphorus and molecular nitrogen. Furnace anneal for the phosphorus only sample is presented again for comparison.

attributed to the higher diffusion of phosphorus when the pulse duration increases. In that case, the sheet resistance ranges from 58 to 68 Ω/□ for the 10 and 8 ms pulse, respectively, values that are typical for this doping level.[15] For the phosphorus and nitrogen co-doping, the sheet resistances are higher ranging from 131 to 153 Ω/□ for 8 and 10 ms.

The performance of the annealed devices as diodes has also been evaluated. Figure 4 presents the I-V characteristics for two diodes annealed with an 8 ms pulse at the specified conditions. Both devices indicate a strong forward bias current at 1 V. There is no significant difference on the currents in forward bias, which is improved over the furnace annealed sample. The co-doping seems to improve the reverse bias leakage by about one order of magnitude in comparison to the phosphorus only sample, but leakage is still higher than the furnace annealed sample. In general, the measured values are in accordance with current literature regarding laser annealed germanium diodes,[16] although not on par with RTA processes. The relevantly high leakage current for the laser annealed samples indicates that deep level defects are

TABLE II. Sheet resistance results.

Doping	Pulse (ms)	Sheet resistance (Ω/□)
P only	8	68 ± 6
P only	10	58 ± 6
P and N_2	8	153 ± 10
P and N_2	10	131 ± 10
P only	30 min–650 °C	62 ± 3

not fully treated by the annealing process and operate as generation centers increasing the leakage current. The reduced leakage current observed in the presence of nitrogen could be attributed to passivation of these centers by nitrogen. We also observe that the higher thermal budget of the furnace anneal is more effective in treating those defects leading to even lower leakage. The same improved leakage behavior has been observed for samples annealed with RTA.[7]

Finally, AFM measurements have been performed to evaluate the surface reconstruction quality of the annealed samples. In Figure 5, AFM micrographs of a sample before and after 10 ms annealing are presented. It is apparent that laser annealing effectively reconstructs the surface of the sample reducing its mean surface roughness from about 35 nm down to less than 2 nm. However, this drop in roughness could indicate a lower melting threshold for the highly amorphous surface regions. Additionally, by comparing the step between the SiO_2 layer and the exposed germanium area before and after the annealing, no measurable substrate loss could be observed.

Using a similar approach with silicon,[6] future work can compare simulation results of the complete laser annealing process with the present experimental data. Another interesting feature could be the investigation of the immunity of long wavelength laser annealing to 2-D effects related with geometrical constraints as it was previously reported for excimer laser annealing[17] by both simulations and experiments.

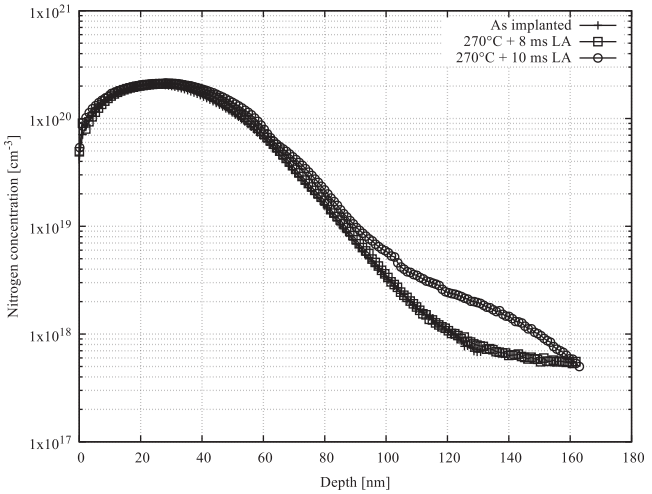

FIG. 3. SIMS nitrogen profiles for 8 and 10 ms laser annealing.

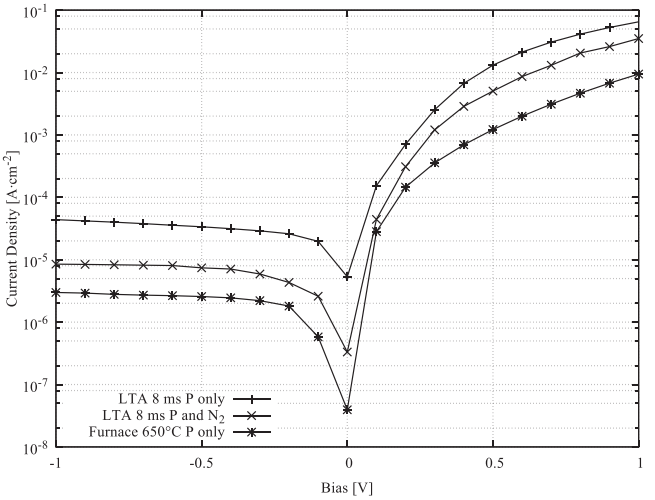

FIG. 4. Diode characteristics for two diodes annealed with 8 ms laser pulse for the two different doping strategies. Furnace annealed sample for comparison.

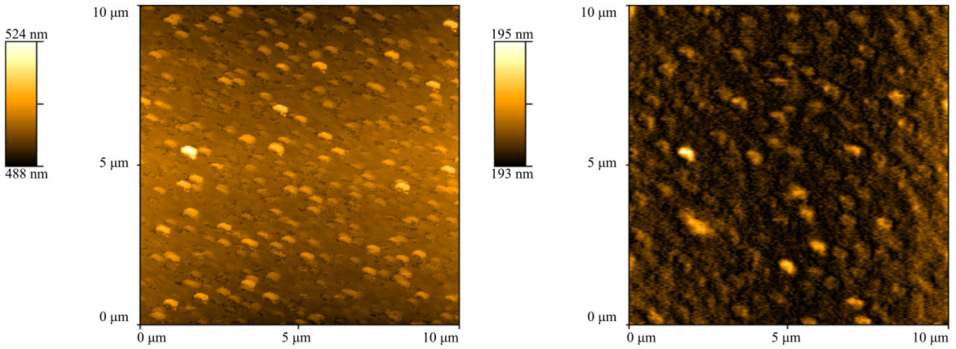

FIG. 5. AFM topography of a sample before (left) and after (right) 10 ms laser annealing.

IV. PHOSPHORUS DIFFUSION SUPPRESSION AND DEACTIVATION DUE TO P-N CLUSTERING

Although the SIMS measurements obviously indicate the improved phosphorus diffusion with the nitrogen co-doping, the higher sheet resistance indicates lower electrical activation. An estimation of the dopant activation can be made by calculating the sheet resistance from the SIMS profile. In order to do so, we utilize the semi-empirical mobility model proposed by Hilsum[18]

$$\mu(x) = \frac{4200}{1 + \sqrt{N(x) \times 1 \times 10^{-17}}}, \quad (1)$$

where $N(x)$ is the total amount of dopant concentration (in cm^{-3}) and x the depth (in cm) within the semiconductor bulk. Thus, from the sheet resistance $R_s = (q \int_0^{x_j} \mu(x) N(x) dx)^{-1}$, where q is the elementary charge and x_j the junction depth, we can estimate the maximum activated phosphorus level at $5.8 \times 10^{19} cm^{-3}$ for the phosphorus only samples, which is close to the maximum level activation levels proposed by other works.[10,19] However, for the co-doped samples, the activation level that corresponds to the measured sheet resistance can be estimated lower to $2.1 \times 10^{19} cm^{-3}$. This indicates that the total activation for the co-doped samples is about 40% of the phosphorus only case. It is apparent that although the diffusion of phosphorus is suppressed, the presence of nitrogen leads to significant deactivation. Higher activation levels have been reported[7] but mostly refer to melting laser annealing and are not directly comparable.

To further elucidate the atomic scale details of phosphorus and nitrogen incorporation in germanium and its effect on diffusion suppression and phosphorus deactivation, we have performed density-functional theory calculations with the plane wave code VASP[20] and projector-augmented potentials.[21] Exchange and correlation effects were described with a generalized-gradient approximation functional.[22] We carried out two sets of calculations on supercells with 64 and 216 germanium atoms (in the defect-free case) to ensure convergence of results. Below, we report only the results based on the 216-atom supercells. The energy cutoff for the plane wave basis was set at 350 eV and the $2 \times 2 \times k$ grid was used in reciprocal space. The criterion for self-consistency in terms of the total energy was set at 10^{-4} eV. Similar methodology has been applied in the past in several defect-related DFT studies on germanium and silicon based systems.[23–25] Previous works have focused mostly on the vacancy-mediated mechanism of phosphorus diffusion in germanium.[2,26,27] In this context, the suppression of phosphorus diffusion can be attributed to the trapping of vacancies at nitrogen dopant sites in germanium. Here, we focus instead on the direct role that the nitrogen co-dopants may have in the stability of phosphorus-related structures in germanium.

In order to assess the relative stability of various N-P impurity complexes, we first examined the structural details and energetics of isolated point defects and impurities in germanium. In particular, we examined various neutral configurations of a germanium self-interstitial and used the relaxed structures to probe the stability of nitrogen and phosphorus interstitials in germanium. The geometries we considered are the so-called (110)- and (100)-split interstitials, the tetrahedral arrangement, and the structure with the self-interstitial at the center of a hexagon of bulk germanium (hexagonal geometry). In agreement with previous studies,[28,29] we found that the (110)-split structure [shown in Figure 6(a)] is the most stable interstitial configuration in bulk germanium.

Likewise, the lowest energy structure for an extra phosphorus atom in the bulk of germanium resembles the (110)-split geometry [Figure 6(b)] with a stretched P-Ge bond length of 2.42 Å for the germanium and phosphorus atoms involved. However, the structure with phosphorus at the center of a hexagon and the (100)-split configuration are very close in energy (0.02 eV and 0.26 eV, respectively), especially the hexagonal geometry is practically degenerate in terms of energy with the (110)-split arrangement. In the case of a nitrogen interstitial, the split geometries are again the most stable configurations, albeit the (100)-split structure [Figure 6(c)] is more stable than the (110) one by 0.16 eV.

There is a high energy penalty of 1.81 eV for a nitrogen interstitial to replace a germanium atom and create thus a nitrogen substitutional impurity and a germanium self-interstitial (at remote distance). In contrast, the same process has a reaction energy of only 0.22 eV in the case of phosphorus, indicating a much stronger tendency for phosphorus to react with defect-free germanium and become a substitutional dopant. However, there are strong energy gains of 2.27 eV and 3.85 eV when a nitrogen or phosphorus interstitial occupies the center of an existing germanium single-vacancy (i.e., without the creation of a germanium interstitial).

When germanium is co-doped with nitrogen and phosphorus, then very stable N-P complexes can be formed. The lowest energy N-P structure at a germanium vacancy site is

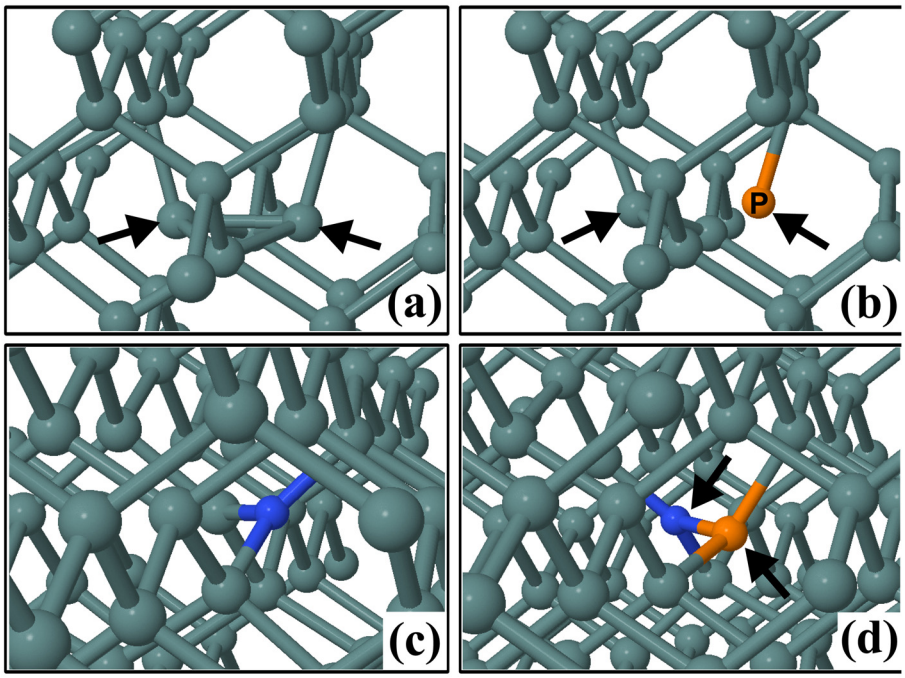

FIG. 6. Defect and impurity configurations in bulk germanium: (a) (110)-split self-interstitial (the two participating germanium atoms shown with arrows), (b) phosphorus interstitial in a (110)-split geometry (the distance between the germanium and phosphorus atoms shown with arrows is 2.42 Å), (c) nitrogen interstitial in a (100)-split configuration, (d) N-P complex in a (100)-split geometry on a germanium vacancy site (dark gray (dark green): germanium, black (blue): nitrogen, gray (orange): phosphorus spheres).

shown in Figure 6(d). Starting from a nitrogen substitutional site and a remote phosphorus interstitial, the creation of the depicted N-P complex releases 2.69 eV. Significant energy (1.11 eV) is gained also when this N-P geometry is formed upon trapping of a nitrogen interstitial by a phosphorus substitutional dopant. These energy gains show that the N-P complexes are formed regardless of the initial configuration. We should also stress that the creation of the N-P complex is also energetically favored (by 0.88 eV) when nitrogen and phosphorus interstitial atoms react to form the geometry of Figure 6(d) through the concurrent ejection of a germanium self-interstitial in the bulk. Finally, by comparing electronic density of states calculations for the defect-free germanium supercell with 216 atoms and a supercell of the same size with an N-P complex inside, we assessed that the N-P complex does not introduce any levels in the energy band gap of the material or close to the valence band and conduction band edges.

Based on the above results, we can conclude that when nitrogen atoms are implanted in phosphorus doped germanium, some of them hinder the diffusion of phosphorus dopants by trapping them in stable N-P clusters. By the same token, the formation of N-P complexes reduces the number of active substitutional phosphorus dopants. Both conclusions are consistent with our main experimental observations.

V. CONCLUSION

In this article, we presented the use of millisecond laser annealing and phosphorus-nitrogen co-doping to fabricate shallow junctions in germanium. Although laser annealing provides a degree of control upon the diffusion of phosphorus, additional diffusion suppression can be achieved by using nitrogen co-doping leading to practically diffusionless junctions. According to the DFT calculations presented, this suppression is an effect of the stable phosphorus-nitrogen complexes that are formed in germanium, which limit the amount of phosphorus that can be diffused, although the amount of electrically active phosphorus is limited. However, it is apparent that through the controlled use of laser annealing, nitrogen co-doping and potentially more advanced implantation techniques, such as ultra low energy and plasma doping, diffusionless junctions with very good electrical characteristics can be obtained.

ACKNOWLEDGMENTS

This research has been co-financed by the European Union (European Social Fund—ESF) and Greek national funds through the Operational Program "Education and Lifelong Learning" of the National Strategic Reference Framework (NSRF)—Research Funding Program: "Heracleitus II. Investing in knowledge society through the European Social Fund" that supports Mr. Stathopoulos. The DFT calculations used resources of the "Hellasgrid" and EGEE infrastructures.

[1]I. Riihimäki, A. Virtanen, S. Rinta-Anttila, P. Pusa, J. Räisänen, and ISOLDE Collaboration, "Vacancy-impurity complexes and diffusion of Ga and Sn in intrinsic and p-doped germanium," Appl. Phys. Lett. **91**(9), 091922 (2007).
[2]S. Brotzmann and H. Bracht, "Intrinsic and extrinsic diffusion of phosphorus, arsenic, and antimony in germanium," J. Appl. Phys. **103**(3), 033508 (2008).
[3]A. Chroneos and H. Bracht, "Diffusion of n-type dopants in germanium," Appl. Phys. Rev. **1**(1), 011301 (2014).
[4]A. Chroneos, "Effect of germanium substrate loss and nitrogen on dopant diffusion in germanium," J. Appl. Phys. **105**(5), 056101 (2009).
[5]R. J. Kaiser, S. Koffel, P. Pichler, A. J. Bauer, B. Amon, L. Frey, and H. Ryssel, "Germanium substrate loss during thermal processing," Microelectron. Eng. **88**(4), 499–502 (2011).
[6]S. Stathopoulos, A. Florakis, G. Tzortzis, T. Laspas, A. Triantafyllopoulos, Y. Spiegel, F. Torregrosa, and D. Tsoukalas, "CO_2 laser annealing for USJ formation in silicon: Comparison of simulation and experiment," IEEE Trans. Electron Devices **61**(3), 696–701 (2014).

[7]M. Shayesteh, D. O'Connell, F. Gity, P. Murphy-Armando, R. Yu, K. Huet, I. Toque-Tresonne, F. Cristiano, S. Boninelli, H. H. Henrichsen, P. F. Nielsen, D. H. Petersen, and R. Duffy, "Optimized laser thermal annealing on germanium for high dopant activation and low leakage current," IEEE Trans. Electron Devices **61**(12), 4047–4055 (2014).
[8]C. Wang, C. Li, S. Huang, W. Lu, G. Yan, M. Zhang, H. Wu, G. Lin, J. Wei, W. Huang, H. Lai, and S. Chen, "Phosphorus diffusion in germanium following implantation and excimer laser annealing," Appl. Surf. Sci. **300**, 208–212 (2014).
[9]L. M. Feng, Y. Wang, and D. A. Markle, "Minimizing pattern dependency in millisecond annealing," in *International Workshop on Junction Technology, IWJT'06* (2006), pp. 25–30.
[10]E. Simoen, A. Satta, A. D'Amore, T. Janssens, T. Clarysse, K. Martens, B. De Jaeger, A. Benedetti, I. Hoflijk, B. Brijs, M. Meuris, and W. Vandervorst, "Ion-implantation issues in the formation of shallow junctions in germanium," Mater. Sci. Semicond. Process. **9**(4–5), 634–639 (2006).
[11]C. Thomidis, M. Barozzi, M. Bersani, V. Ioannou-Sougleridis, N. Z. Vouroutzis, B. Colombeau, and D. Skarlatos, "Strong diffusion suppression of low energy-implanted phosphorous in germanium by N_2 Co-implantation," ECS Solid State Lett. **4**(6), P47–P50 (2015).
[12]H. A. W. El Mubarek, "Reduction of phosphorus diffusion in germanium by fluorine implantation," J. Appl. Phys. **114**(22), 223512 (2013).
[13]A. Florakis, E. Verrelli, D. Giubertoni, G. Tzortzis, and D. Tsoukalas, "Non-melting annealing of silicon by CO_2 laser," Thin Solid Films **518**(9), 2551–2554 (2010).
[14]P. Tsouroutas, D. Tsoukalas, A. Florakis, I. Zergioti, A. A. Serafetinides, N. Cherkashin, B. Marty, and A. Claverie, "Laser annealing for n+/p junction formation in germanium," Mater. Sci. Semicond. Process. **9**(4–5), 644–649 (2006).
[15]P. Tsouroutas, D. Tsoukalas, and H. Bracht, "Experiments and simulation on diffusion and activation of codoped with arsenic and phosphorous germanium," J. Appl. Phys. **108**(2), 024903 (2010).
[16]C. Wang, C. Li, G. Lin, W. Lu, J. Wei, W. Huang, H. Lai, S. Chen, Z. Di, and M. Zhang, "Germanium n+/p shallow junction with record rectification ratio formed by low-temperature preannealing and excimer laser annealing," IEEE Trans. Electron Devices **61**(9), 3060–3065 (2014).
[17]A. La Magna, P. Alippi, V. Privitera, S. Scalese, S. Pannitteri, G. Fortunato, L. Mariucci, and M. Camalleri, "Material modifications induced by laser annealing in two-dimensional structures," Appl. Phys. Lett. **84**(23), 4738 (2004).
[18]C. Hilsum, "Simple empirical relationship between mobility and carrier concentration," Electron. Lett. **10**(13), 259–260 (1974).
[19]N. S. Bennett and N. E. B. Cowern, "Doping characterization for germanium-based microelectronics and photovoltaics using the differential hall technique," Appl. Phys. Lett. **100**(17), 172106 (2012).
[20]G. Kresse and D. Joubert, "From ultrasoft pseudopotentials to the projector augmented-wave method," Phys. Rev. B **59**(3), 1758–1775 (1999).
[21]P. E. Blöchl, "Projector augmented-wave method," Phys. Rev. B **50**(24), 17953–17979 (1994).
[22]J. P. Perdew and Y. Wang, "Accurate and simple analytic representation of the electron-gas correlation energy," Phys. Rev. B **45**(23), 13244–13249 (1992).
[23]L. Tsetseris and S. T. Pantelides, "Morphology and defect properties of the Ge–GeO_2 interface," Appl. Phys. Lett. **95**(26), 262107 (2009).
[24]L. Tsetseris, D. M. Fleetwood, R. D. Schrimpf, X. J. Zhou, I. G. Batyrev, and S. T. Pantelides, "Hydrogen effects in MOS devices," Microelectron. Eng. **84**(9–10), 2344–2349 (2007).
[25]L. Tsetseris, S. Wang, and S. T. Pantelides, "Thermal donor formation processes in silicon and the catalytic role of hydrogen," Appl. Phys. Lett. **88**(5), 051916 (2006).
[26]J. Coutinho, S. Öberg, V. J. B. Torres, M. Barroso, R. Jones, and P. R. Briddon, "Donor-vacancy complexes in Ge: Cluster and supercell calculations," Phys. Rev. B **73**(23), 235213 (2006).
[27]A. Chroneos, H. Bracht, R. W. Grimes, and B. P. Uberuaga, "Vacancy-mediated dopant diffusion activation enthalpies for germanium," Appl. Phys. Lett. **92**(17), 172103 (2008).
[28]A. J. R. da Silva, A. Janotti, A. Fazzio, R. J. Baierle, and R. Mota, "Self-interstitial defect in germanium," Phys. Rev. B **62**(15), 9903–9906 (2000).
[29]M. Dionízio Moreira, R. H. Miwa, and P. Venezuela, "Electronic and structural properties of germanium self-interstitials," Phys. Rev. B **70**(11), 115215 (2004).